nature portfolio

https://doi.org/10.1038/s41560-022-01055-0

Supplementary information

Low-solvation electrolytes for high-voltage sodium-ion batteries

In the format provided by the authors and unedited

Supplementary information

Low-solvation electrolytes for high-voltage sodium-ion batteries

Yan Jin[1], Phung M. L. Le[1], Peiyuan Gao[2], Yaobin Xu[3], Biwei Xiao[1], Mark H. Engelhard[3], Xia Cao[1], Thanh D. Vo[1], Jiangtao Hu[1], Lirong Zhong[1], Bethany E. Matthews[1], Ran Yi[1], Chongmin Wang[3], Xiaolin Li[1], Jun Liu[1, 4], Ji-Guang Zhang[1, *]

1: Energy and Environment Directorate, Pacific Northwest National Laboratory, Richland, Washington 99352, USA

2. Physical and Computational Sciences Directorate, Pacific Northwest National Laboratory, Richland, Washington 99352, USA

3: Environmental Molecular Sciences Laboratory, Pacific Northwest National Laboratory, Richland, Washington 99352, USA

4. Materials Science and Engineering Department, University of Washington, Seattle, Washington 98105, USA

* Corresponding Author: Ji-Guang Zhang: jiguang.zhang@pnnl.gov

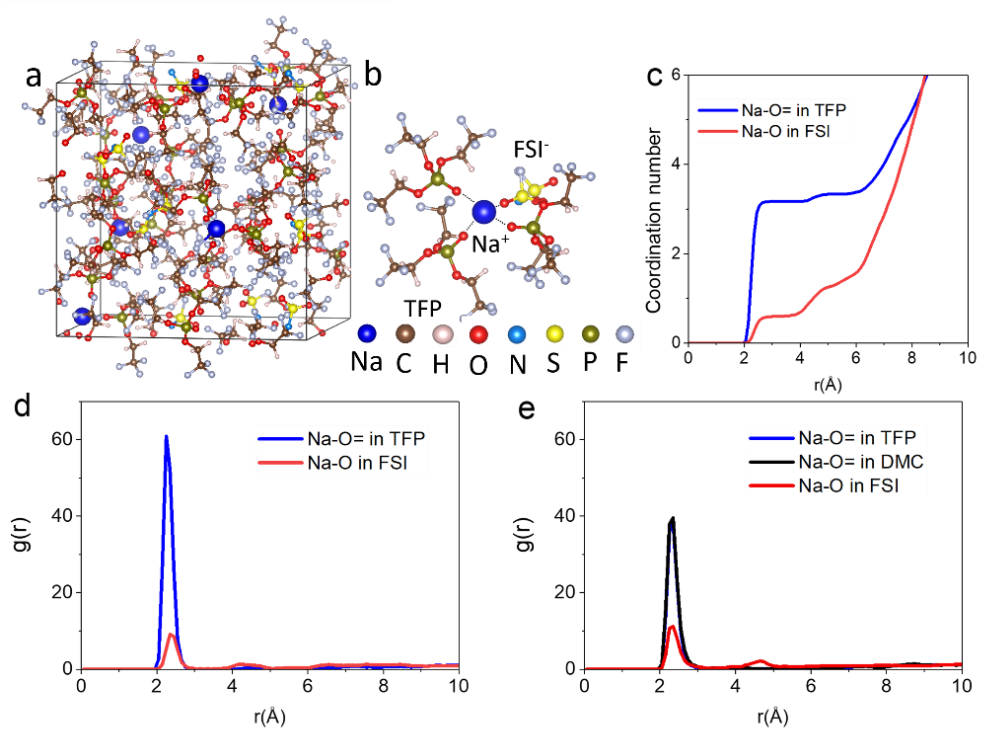

Supplementary Figure 1 | Ab initio molecular dynamics (AIMD) simulation snapshots (a), the representative Na^+ solvation structure extracted from the AIMD simulations (b), coordination number (c) and the corresponding radial distribution functions (d, e) of NaFSI/TFP (a-d) and NaFSI/DMC:TFP electrolytes (e).

Supplementary Note 1 | In a NaFSI/TFP electrolyte, average 3.35 TFP molecules and 0.65 FSI^- molecules coordinate with Na^+ (Supplementary Fig. 1c). However, in a NaFSI/DMC:TFP electrolyte, average 1.65 TFP molecules,1.35 DMC molecules, and 1.25 FSI^- molecules coordinate with Na^+ (Fig. 1h).

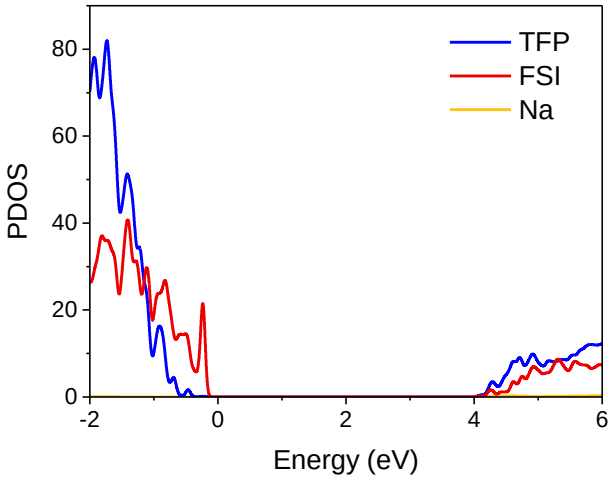

Supplementary Figure 2 | AIMD simulation: the projected density of states (PDOS) of NaFSI/TFP electrolyte.

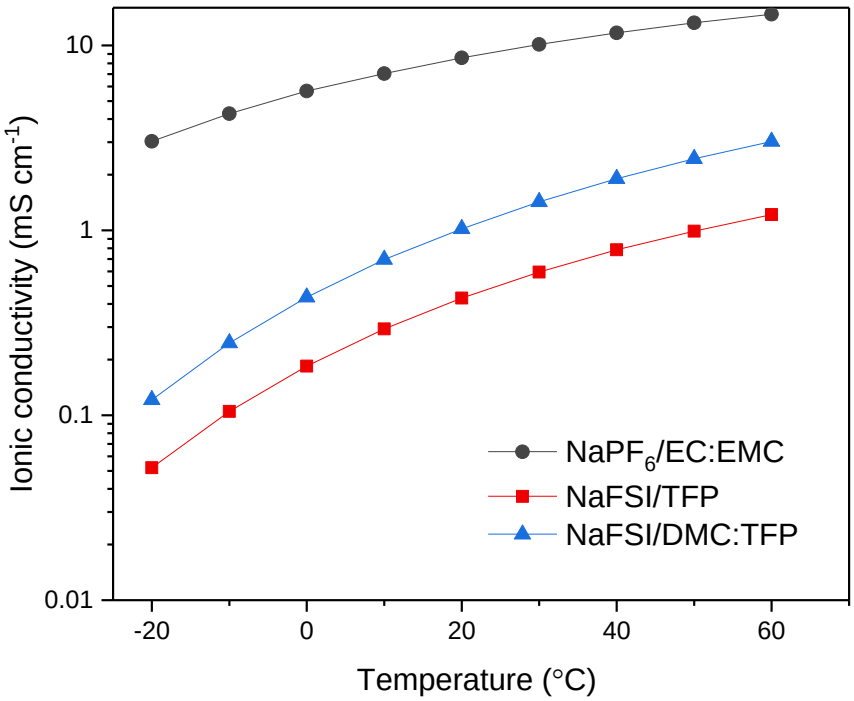

Supplementary Figure 3 | Temperature dependence of ionic conductivities from -20 to 60 °C.

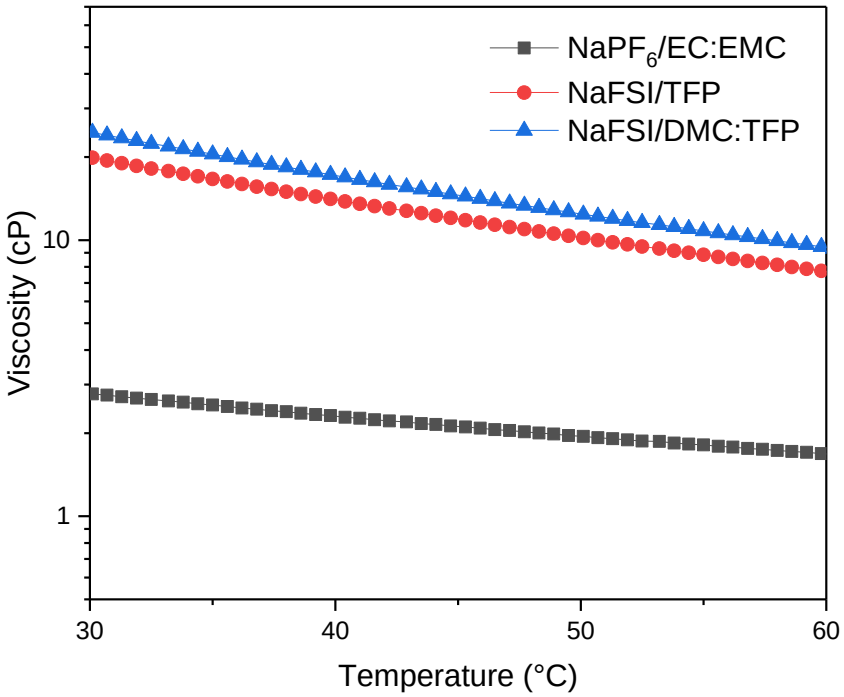

Supplementary Figure 4 | Viscosity of three electrolytes in the temperature range of 30-60 °C.

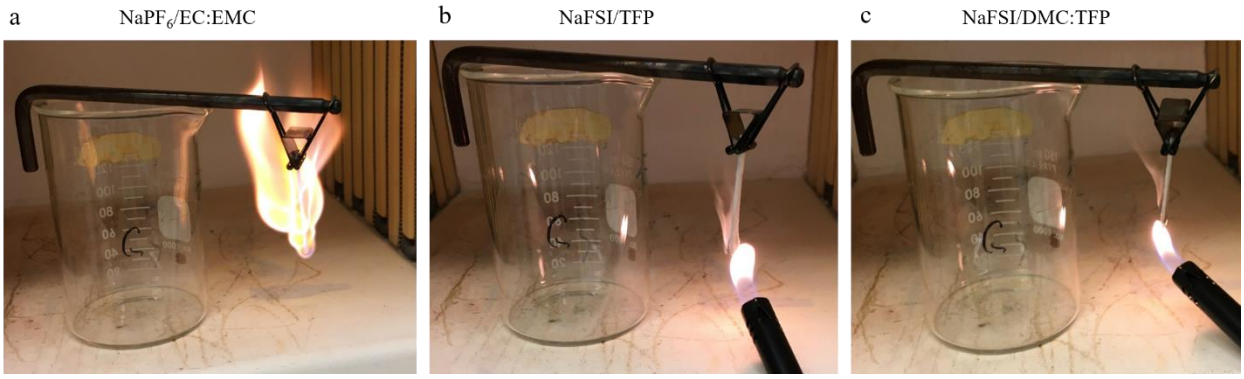

Supplementary Figure 5 | Flammability test of three electrolytes.

Supplementary Note 2 | Carbonate $NaPF_6$/EC:EMC electrolyte is flammable with a self-extinguish time of 49 s g^{-1}. In contrast, NaFSI/TFP electrolyte is not ignited because of the nonflammable TFP solvent. When heated, the released P-based radical from pyrolysis of TFP can neutralize the hydrogen and oxygen-based radicals that are indispensable for combustion. NaFSI/DMC:TFP electrolyte is also nonflammable because of large amount of TFP (84 wt%).

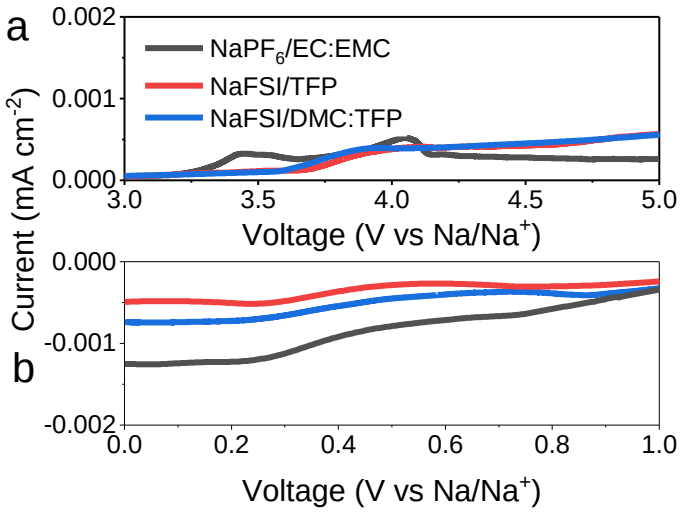

Supplementary Figure 6 | Oxidation (a) and reduction (b) stability of three electrolytes (enlarged curves of Fig. 2a).

Supplementary Note 3 | There is no apparent onset of oxidation current for $NaPF_6$/EC:EMC carbonate electrolyte on Al substrate, which is consistent with previous published results,[1,2] suggesting a stable passivation layer that inhibits the Al corrosion and electrolyte decomposition on Al.[3] These tiny peaks at around 3.5 and 4 V generated at a very slow scan rate of 0.05 mV s^{-1} are originated from the formation of a passivation layer on the Al current collector and/or oxidation of impurities, which agrees well with the previous published results.[3,4] TFP based electrolytes also show good oxidation stability up to 5 V, which can meet the requirement for high voltage cell with cutoff voltage of 4.2 V.

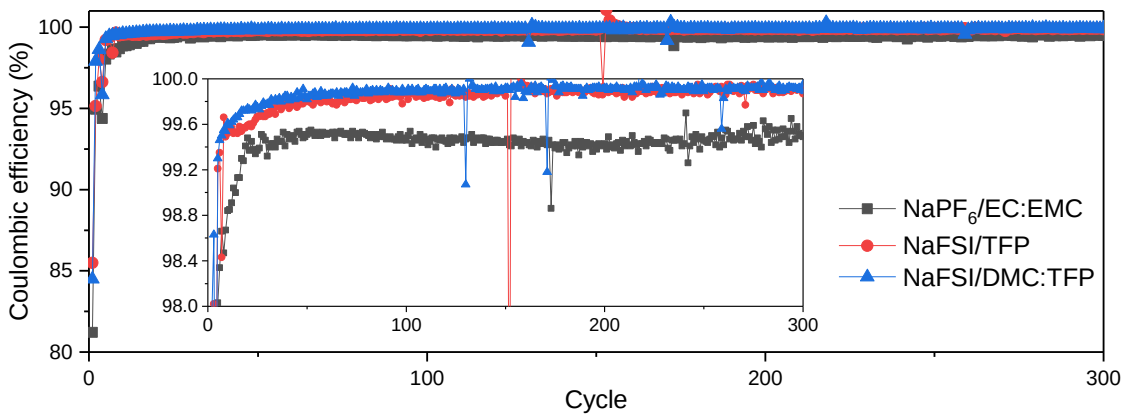

Supplementary Figure 7 | Coulombic efficiency (CE) of hard carbon (HC)||$NaNi_{0.68}Mn_{0.22}Co_{0.1}O_2$ (NaNMC) full cells during the long-term cycling using three electrolytes cycled at 0.2 C after three formation cycles at 0.1 C. The NaNMC loading is 1.5 mAh cm^{-2}. Inset shows the zoom-in view of CE.

Supplementary Note 4 | Average CE of HC||NaNMC full cells is ~ 99.45% for $NaPF_6$/EC:EMC, ~ 99.84% for NaFSI/TFP, and ~ 99.89% for NaFSI/DMC:TFP electrolyte (from 10th to 300th cycles), respectively. Although the absolute value of the measured CE is limited by the resolution of the test instrument (especially when CE is > 99.5%), CE of HC||NaNMC full cells in the NaFSI/DMC:TFP electrolyte is clearly higher than those in the $NaPF_6$/EC:EMC electrolyte.

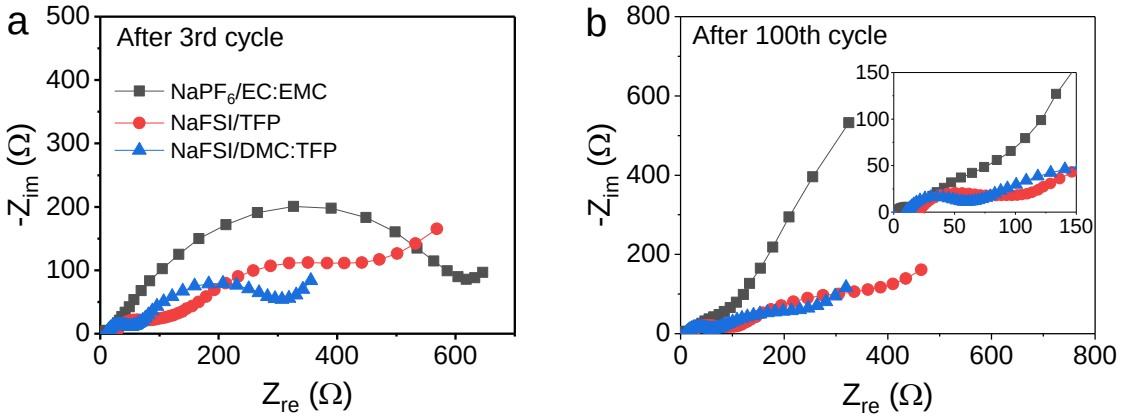

Supplementary Figure 8 | Nyquist plots of HC||NaNMC cells using $NaPF_6$/EC:EMC, NaFSI/TFP and NaFSI/DMC:TFP electrolytes after 3rd (a) and 100th (b) cycles. Inset in b is the enlarged Nyquist plots of the high-frequency region.

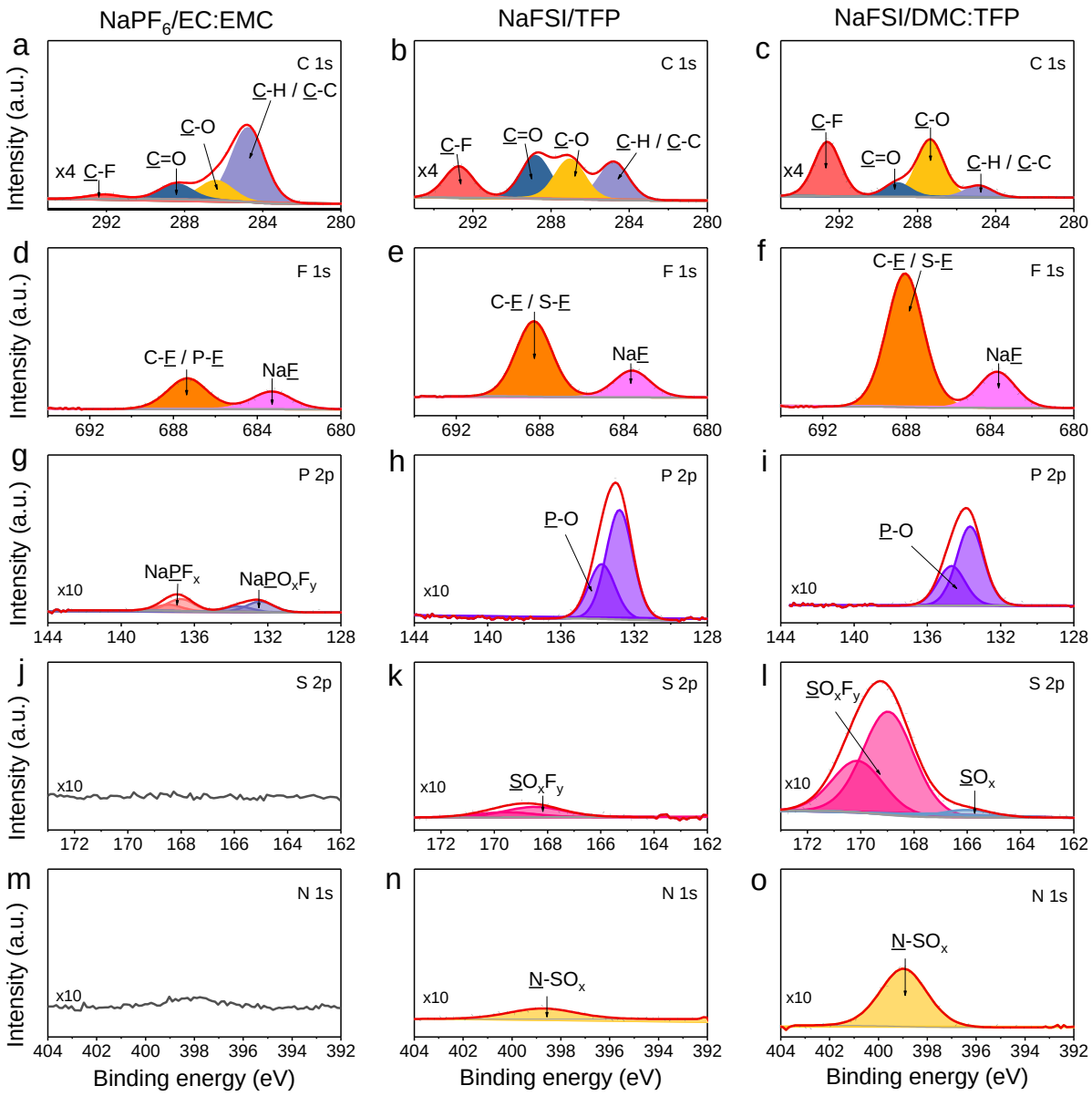

Supplementary Figure 9 | XPS characterization of the SEI components on cycled hard carbon anodes. a-o, XPS spectra of C 1s (a-c), F 1s (d-f), P 2p (g-i), S 2p (j-l) and N 1s (m-o) of the hard carbon anodes after 100 cycles in $NaPF_6$/EC:EMC (a, d, g, j, m), NaFSI/TFP (b, e, h, k, n) and NaFSI/DMC:TFP (c, f, i, l, o) electrolytes (signal depth = 0 nm). Note: upper parts of Fig. 3 b, c, e, f are plotted here as Supplementary Fig. 9 a, g, b, n for parallel comparison.

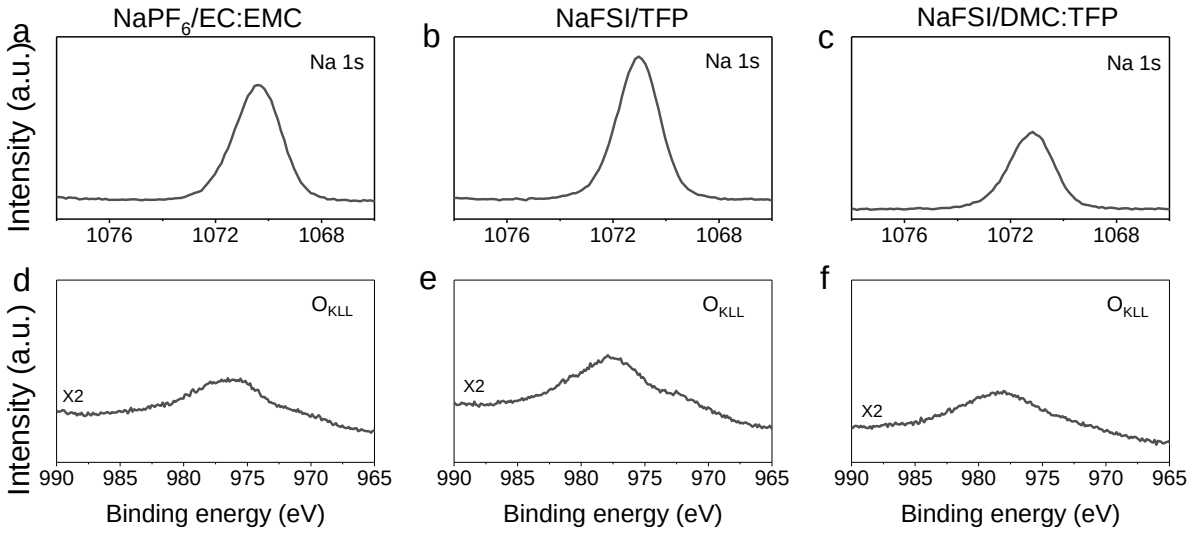

Supplementary Figure 10 | XPS characterization of the SEI components on cycled hard carbon anodes. a-f, XPS spectra of Na 1s (a-c) and O_{KLL} (d-f) of the hard carbon anodes after 100 cycles in $NaPF_6$/EC:EMC (a, d), NaFSI/TFP (b, e) and NaFSI/DMC:TFP (c, f) electrolytes (signal depth = 0 nm).

Supplementary Note 5 | SEI components analysis.

The C 1s and P 2p spectra were firstly analyzed as representatives of the solvent decomposition (in TFP-based electrolytes). Supplementary Fig. 9a shows that SEI layer formed in $NaPF_6$/EC:EMC electrolyte contains C-C/C-H, C-O, C=O peaks and a weak C-F peak from the carbonate solvent decomposition, which is very similar to C 1s spectra of the pristine hard carbon electrode (Supplementary Fig. 14a). Noting that the elements with underlines represent the atoms of interest in the identified species. However, in NaFSI/TFP electrolyte, lower C-C/C-H peak, higher C-O, C=O peaks and a high C-F peak at ~293 eV are observed (Supplementary Fig. 9b). In NaFSI/DMC:TFP electrolyte, the C-C/C-H and C=O peaks are further suppressed with the even stronger C-F peak (Supplementary Fig. 9c). The strong C-F peak is derived from TFP solvent and

NaFSI salt decomposition. The P 2p peaks originated from the TFP solvent decomposition are observed in both NaFSI/TFP (Supplementary Fig. 9h) and NaFSI/DMC:TFP electrolytes (Supplementary Fig. 9i). Further comparing F 1s spectra in three electrolytes (Supplementary Fig. 9d-f), the order of total F-peak intensity in three electrolytes is as following: $NaPF_6$/EC:EMC < NaFSI/TFP < NaFSI/DMC:TFP. The depth profiles of F 1s in three electrolytes are shown in Supplementary Fig. 11, with the intensity of the Na<u>F</u> peak gradually increased while other C-<u>F</u>/P-<u>F</u>/S-<u>F</u> peak decreased during sputtering. Since NaF is a critical component in a highly stable SEI layer, higher F intensity (corresponding to NaF) observed in the SEI layer formed in NaFSI/DMC:TFP electrolyte indicates that the SEI is rich in NaF component, which will lead to more stable cell performance.

Furthermore, the inorganic components from salt decomposition were also compared, with P 2p from $NaPF_6$ in $NaPF_6$/EC:EMC electrolyte and S 2p and N 1s from NaFSI in both NaFSI/TFP and NaFSI/DMC:TFP electrolytes. In P 2p spectrum of $NaPF_6$/EC:EMC electrolyte, the weak Na<u>P</u>F_x and Na<u>P</u>O_xF_y peaks mean less $NaPF_6$ salt decomposition (Supplementary Fig. 9g). The intensity of both S 2p and N 1s peaks is higher in NaFSI/DMC:TFP electrolyte (Supplementary Fig. 9l, o) compared with NaFSI/TFP electrolyte (Supplementary Fig. 9k, n), indicating more NaFSI salt decomposition in NaFSI/DMC:TFP electrolyte.

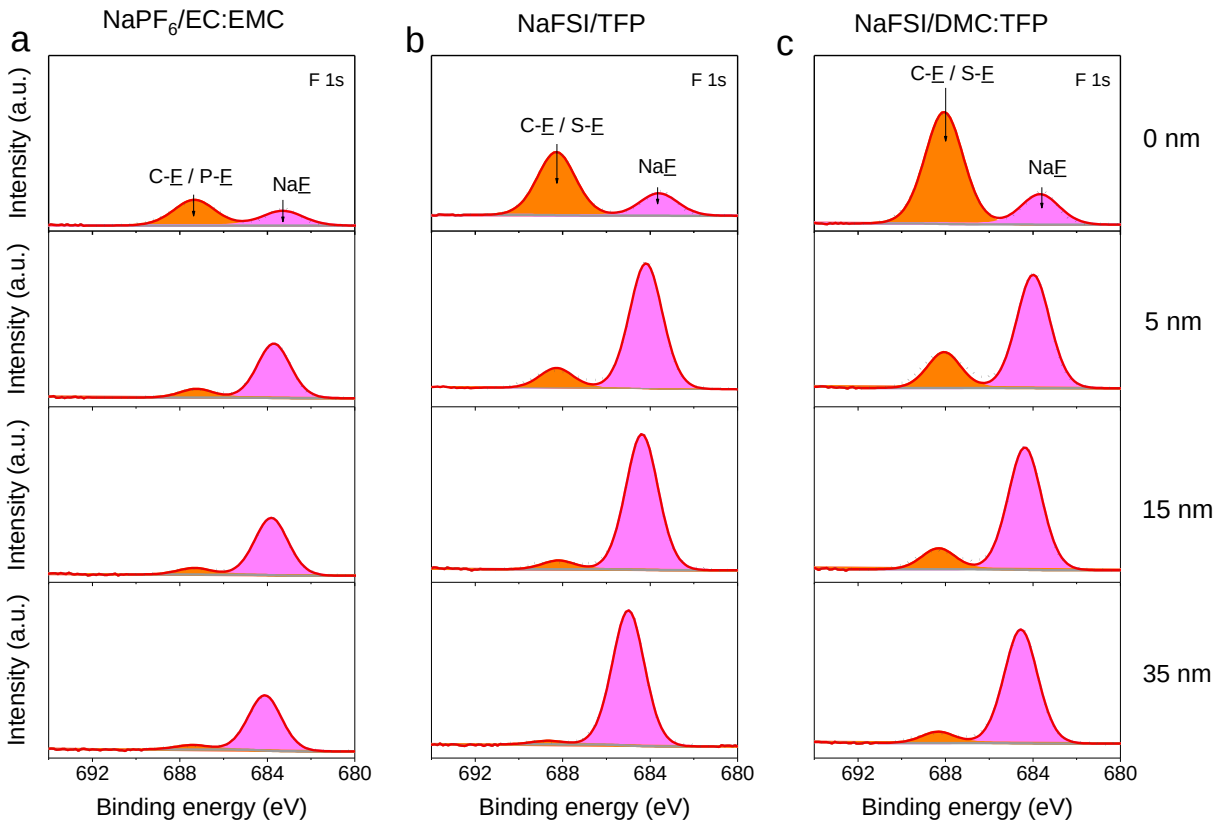

Supplementary Figure 11 | XPS characterization of the SEI components on cycled hard carbon anodes. a-c, XPS depth profile of F 1s of the hard carbon anodes after 100 cycles in $NaPF_6$/EC:EMC (a), NaFSI/TFP (b) and NaFSI/DMC:TFP (c) electrolytes.

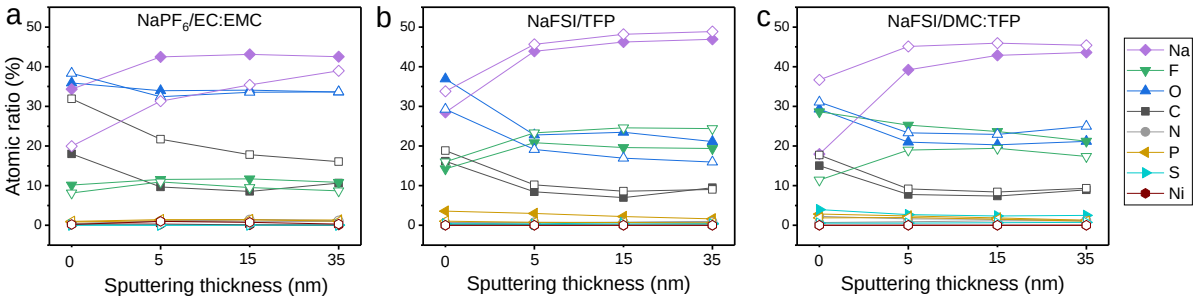

Supplementary Figure 12 | Quantified atomic composition ratios of the SEI obtained by XPS spectra for the hard carbon anodes cycled in $NaPF_6$/EC:EMC (a), NaFSI/TFP (b) and NaFSI/DMC:TFP (c) electrolytes after 100 cycles. Solid symbols represent the cycled hard carbon anodes and hollow symbols were collected from cycled-soaked hard carbon anodes (soaking cycled hard carbon electrodes with solvent of each electrolyte for 50 h).

Supplementary Note 6 | There is some technical difficulty in identifying the SEI solubility in NaFSI/DMC:TFP electrolyte through a soaking experiment by XPS with two reasons. First, the atomic ratio changes of HC soaking in DMC/TFP solvent (Supplementary Fig. 12c) may not fully represent the real case because cycled-soaked electrodes used for XPS are only soaked in DMC:TFP solvent (16 wt% DMC co-solvent can dissolve the SEI) rather than in NaFSI/DMC:TFP electrolyte (with less free-solvent participating in SEI dissolving). Second, the atomic ratio changes of HC soaking in NaFSI/DMC:TFP electrolyte can be interfered by salt decomposition during soak as explained in Supplementary Fig. 13. Indeed, the SEI dissolution is believed to be further suppressed in NaFSI/DMC:TFP electrolyte owing to more salt derived SEI components with less solubility, and unique saturated solvation structure with less free-solvents.

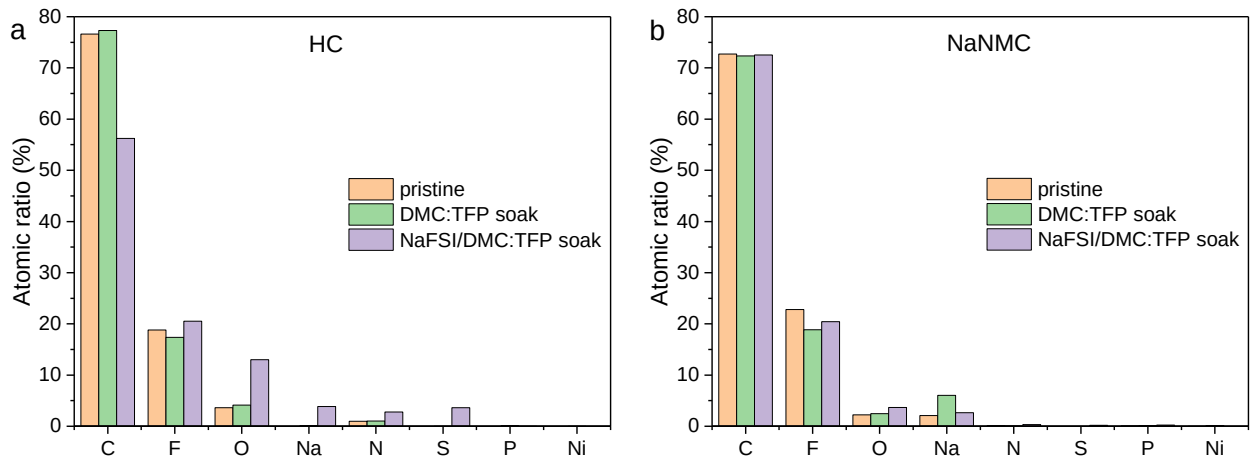

Supplementary Figure 13 | Quantified atomic composition ratios of HC and NaNMC surface at 3 different conditions: pristine, soaked in DMC:TFP solvent and soaked in NaFSI/DMC:TFP electrolyte for 50 h.

Supplementary Note 7 | Interferences from the salt decomposition during soaking experiment, which may interfere the analysis accuracy of SEI dissolution, can be proved by comparing XPS data of pristine electrodes with two kinds of soaked-noncycled electrodes, in Supplementary Fig. 13-15. By comparing the atomic ratio and high resolution XPS spectra, pristine HC soaked in the solvent of DMC:TFP does not show any obvious change compared with the pristine HC. However, for pristine HC soaked in NaFSI/DMC:TFP electrolyte, obvious Na/N/S atomic ratio increasement and the specific XPS spectra presented in Supplementary Fig. 14g-i indicate the electrolyte decomposition from NaFSI salt during the soak period.

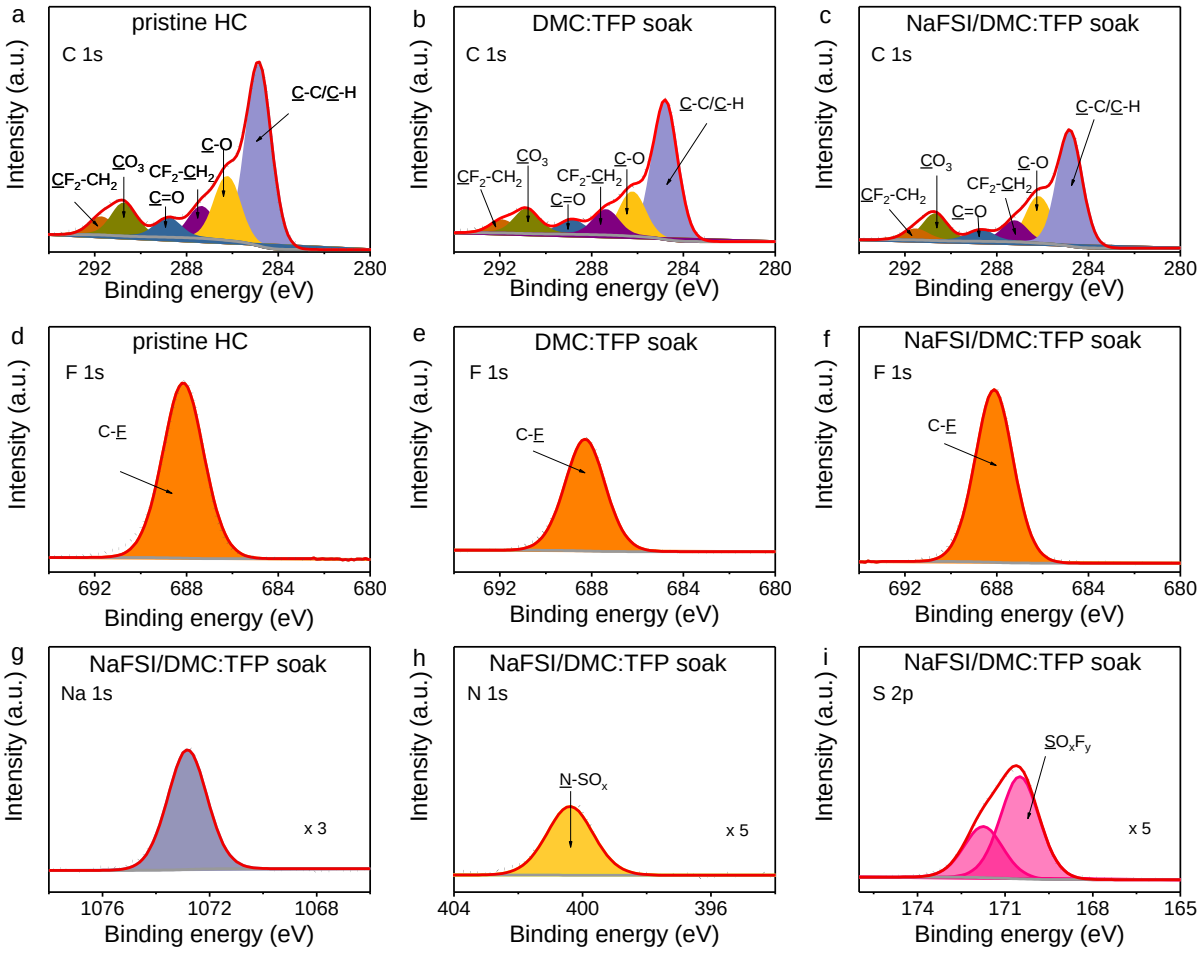

Supplementary Figure 14 | XPS spectra of HC anodes at 3 different conditions: pristine, soaked in DMC:TFP solvent and soaked in NaFSI/DMC:TFP electrolyte for 50 h. a-i, XPS spectra of C 1s (a-c), F 1s (d-f), Na 1s (g), N 1s (h), S 2p (i) of the pristine HC (a, d), HC soaked in DMC:TFP solvent for 50 h (b, e), HC soaked in NaFSI/DMC:TFP electrolyte for 50 h (c, f, g, h, i).

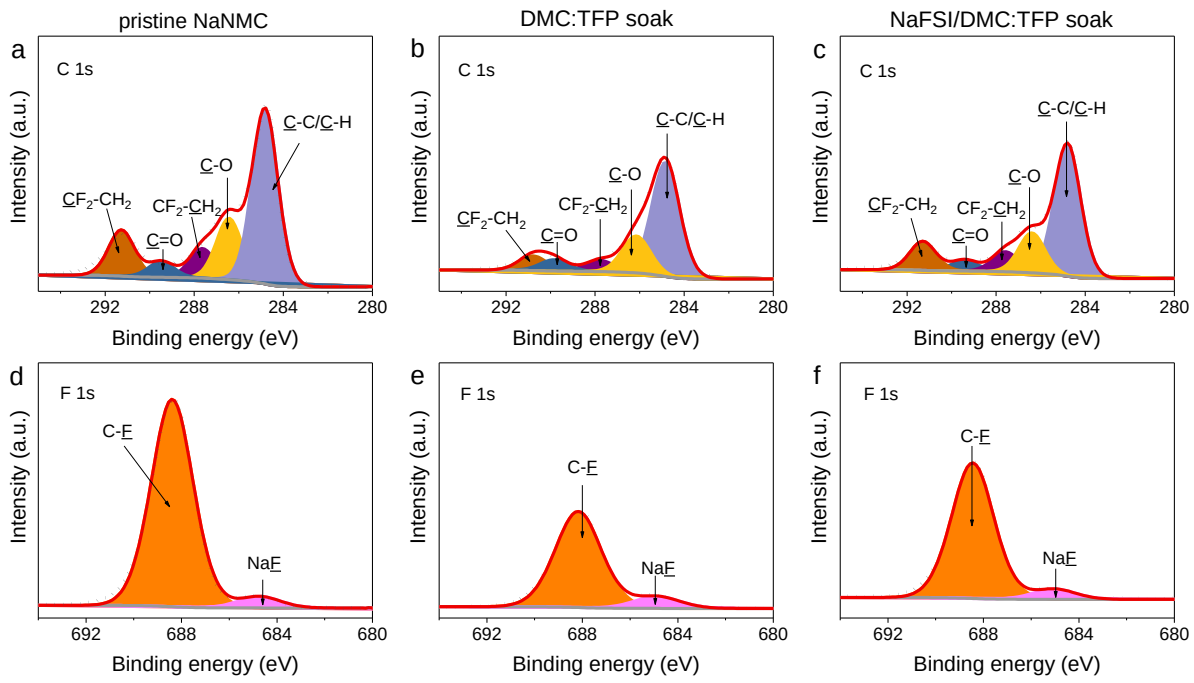

Supplementary Figure 15 | XPS spectra of NaNMC cathodes at 3 different conditions: pristine, soaked in DMC:TFP solvent and soaked in NaFSI/DMC:TFP electrolyte for 50 h. a-f, XPS spectra of C 1s (a-c), F 1s (d-f) of the pristine NaNMC (a, d), NaNMC soaked in DMC:TFP solvent for 50 h (b, e), NaNMC soaked in NaFSI/DMC:TFP electrolyte for 50 h (c, f).

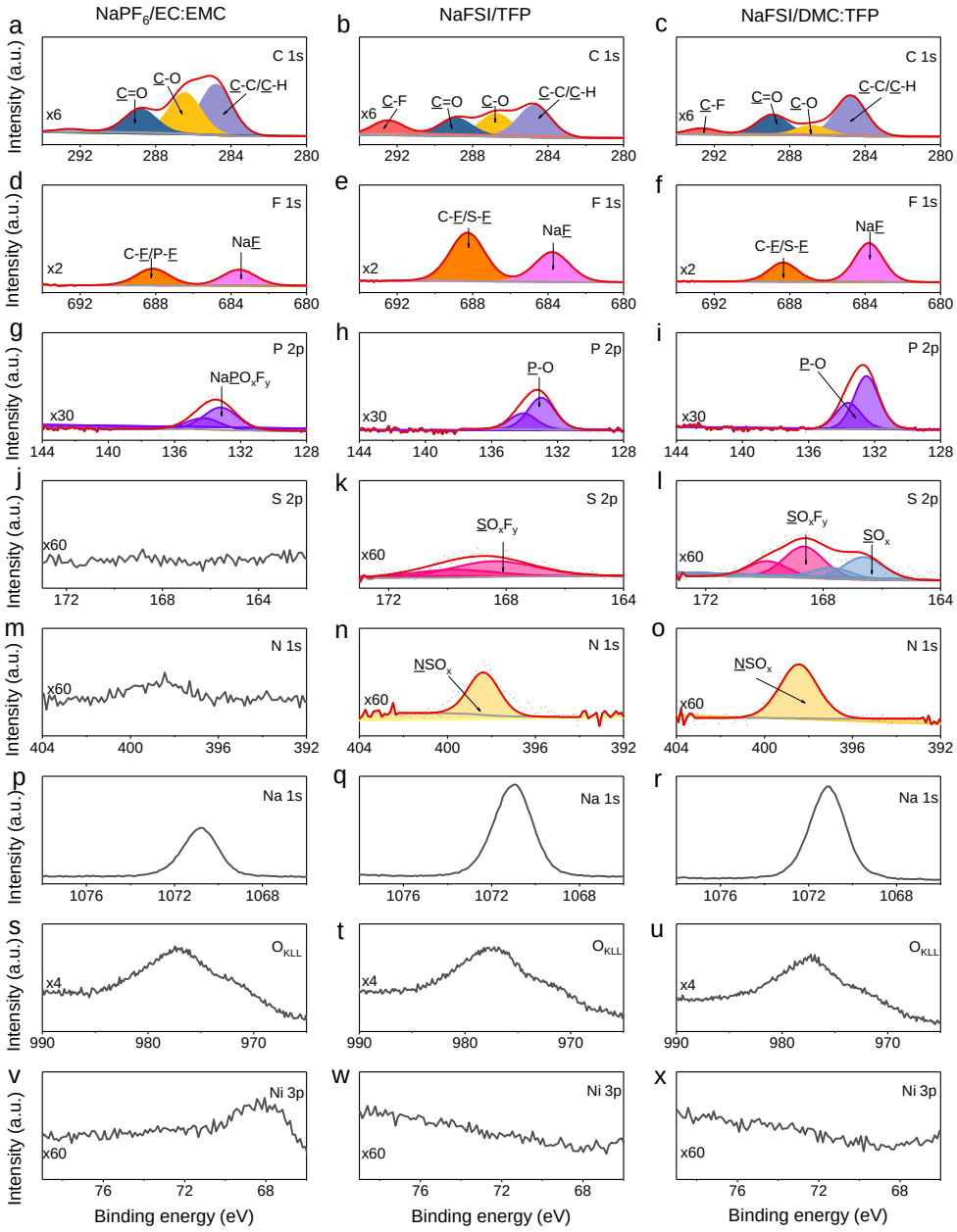

Supplementary Figure 16 | XPS characterization of the SEI components on cycled-soaked hard carbon anodes. a-x, XPS spectra of C 1s (a-c), F 1s (d-f), P 2p (g-i), S 2p (j-l), N 1s (m-o), Na 1s (p-r), O_{KLL} (s-u) and Ni 3p (v-x) of the cycled-soaked hard carbon anodes after 100 cycles in $NaPF_6$/EC:EMC (a, d, g, j, m, p, s, v), NaFSI/TFP (b, e, h, k, n, q, t, w) and NaFSI/DMC:TFP (c, f, i, l, o, r, u, x) electrolytes (signal depth = 0 nm). Note: bottom parts of Fig. 3 b, c, e, f are plotted here as Supplementary Fig. 16 a, g, b, n for parallel comparison.

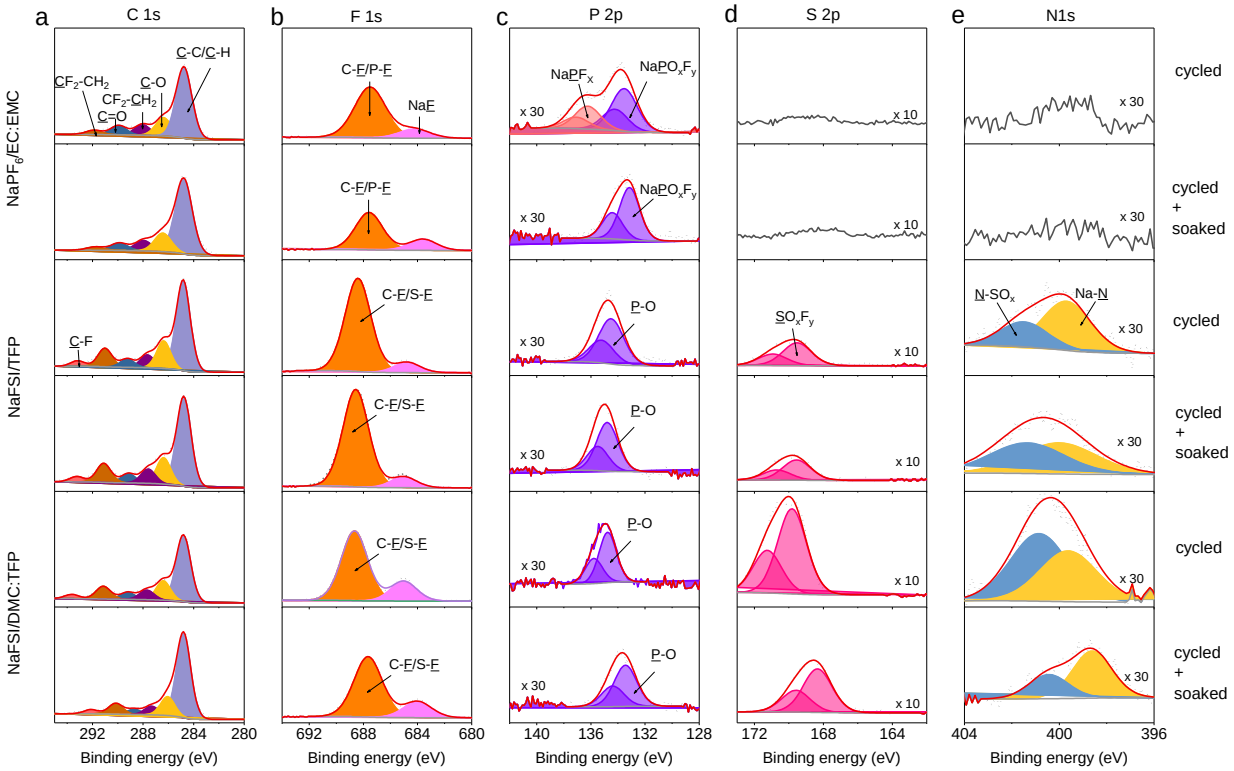

Supplementary Figure 17 | XPS characterization of the CEI components on cycled and cycled-soaked NaNMC cathodes. a-e, XPS spectra of C 1s (a), F 1s (b), P 2p (c), S 2p (d), N 1s (e) of the cycled and cycled-soaked NaNMC cathodes after 100 cycles in $NaPF_6$/EC:EMC, NaFSI/TFP and NaFSI/DMC:TFP electrolytes (signal depth = 0 nm). Note: Fig. 5 a, b, c are plotted here as Supplementary Fig.17 c-$NaPF_6$/EC:EMC-cycled, d-NaFSI/TFP-cycled and d-NaFSI/DMC:TFP-cycled for parallel comparison.

Supplementary Note 8 | CEI component analysis.

C 1s peaks in three electrolytes (Supplementary Fig. 17a) show a tiny difference compared with C 1s spectra of pristine NaNMC (Supplementary Fig. 15a). However, TFP solvent decomposition forms more F components in NaFSI/TFP and NaFSI/DMC:TFP electrolytes (Supplementary Fig.

17b). Besides, the components from salt decomposition are different in three electrolytes. In $NaPF_6$/EC:EMC electrolyte, the weak P 2p peak was derived from $NaPF_6$ salt decomposition (Supplementary Fig. 17c). In NaFSI/TFP electrolyte, there is also S 2p peak from NaFSI salt decomposition (Supplementary Fig. 17d), with the intensity a little bit higher than P 2p peak in baseline $NaPF_6$/EC:EMC electrolyte. In contrast, in NaFSI/DMC:TFP electrolyte, the S 2p peak shows much higher intensity (Supplementary Fig. 17d), indicating much more NaFSI salt decomposition for inorganic components on NaNMC surface. Apart from S 2p peaks, the intensity of N 1s peak in NaFSI/DMC:TFP electrolyte is also higher than NaFSI/TFP electrolyte (Supplementary Fig. 17e), which also confirms more NaFSI salt decomposition for inorganic CEI components in NaFSI/DMC:TFP electrolyte.

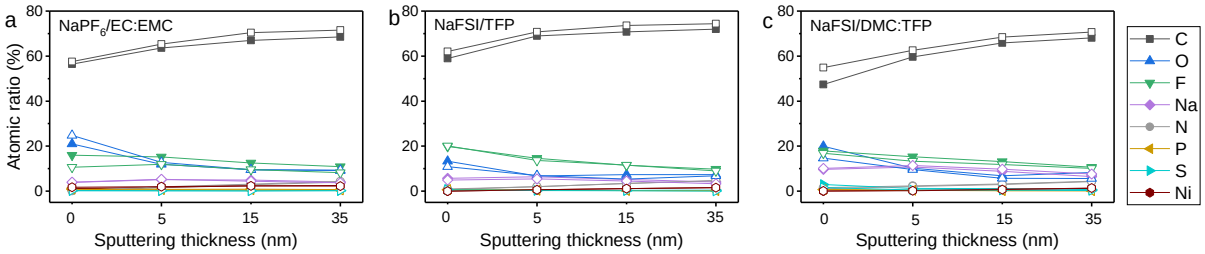

Supplementary Figure 18 | Quantified atomic composition ratios of the CEI from the XPS spectra shown in Supplementary Fig. 17 for the NaNMC cathodes collected from cells in $NaPF_6$/EC:EMC (a), NaFSI/TFP (b) and NaFSI/DMC:TFP (c) electrolytes after 100 cycles. Solid symbols represent the cycled NaNMC cathodes and hollow symbols were collected from cycled-soaked NaNMC cathodes (soaking cycled NaNMC electrodes with solvent of each electrolyte for 50 h).

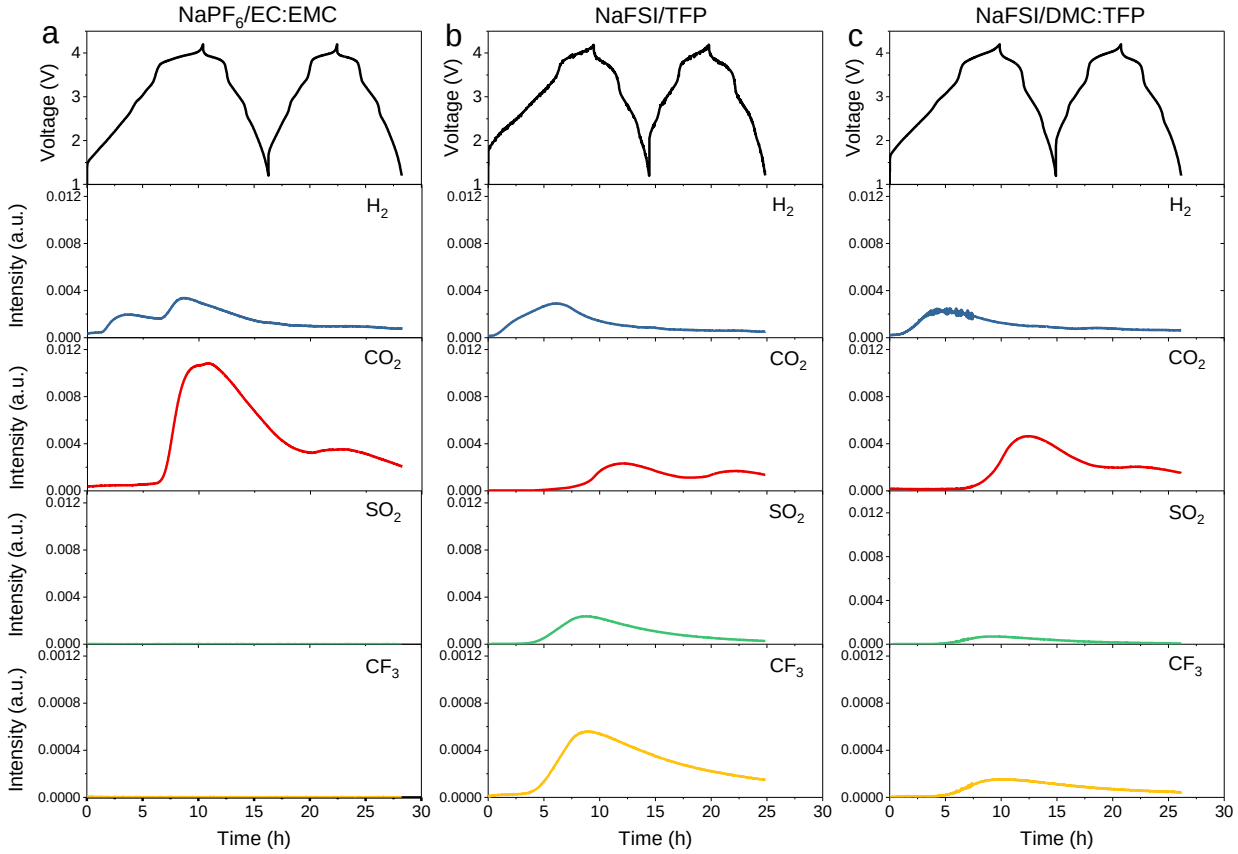

Supplementary Figure 19 | Gas evolution of HC||NaNMC cells with three electrolytes during initial two cycles. The gas generation rate inside the cell was compared by normalized intensity ($Torr_{target\ gas}/Torr_{Ar}$).

Supplementary Note 9 | The gas generation was also suppressed in the NaFSI/DMC:TFP electrolyte as shown in Supplementary Fig. 19. In situ differential electrochemical mass spectrometry (DEMS) measurement was tested for HC||NaNMC cells with three electrolytes during initial two cycles. There are two possible reasons for H_2 evolution. One is the reduction of protic species $R\text{-}H^+$, produced by anodic electrolyte oxidation; the other is H_2O reduction[5,6]. In carbonate baseline electrolyte, strong CO_2 gas formation from carbonate solvent was found in the

first cycle. In NaFSI/TFP electrolyte, the CO_2 formation was suppressed. Meanwhile, there were weak SO_2 from NaFSI salt and relatively small amount of CF_3 from TFP solvent decomposition. In NaFSI/DMC:TFP electrolyte, the gas formation behavior was similar with NaFSI/TFP electrolyte, while the intensity of SO_2 and CF_3 was further suppressed, indicating higher stability of NaFSI and TFP, respectively.

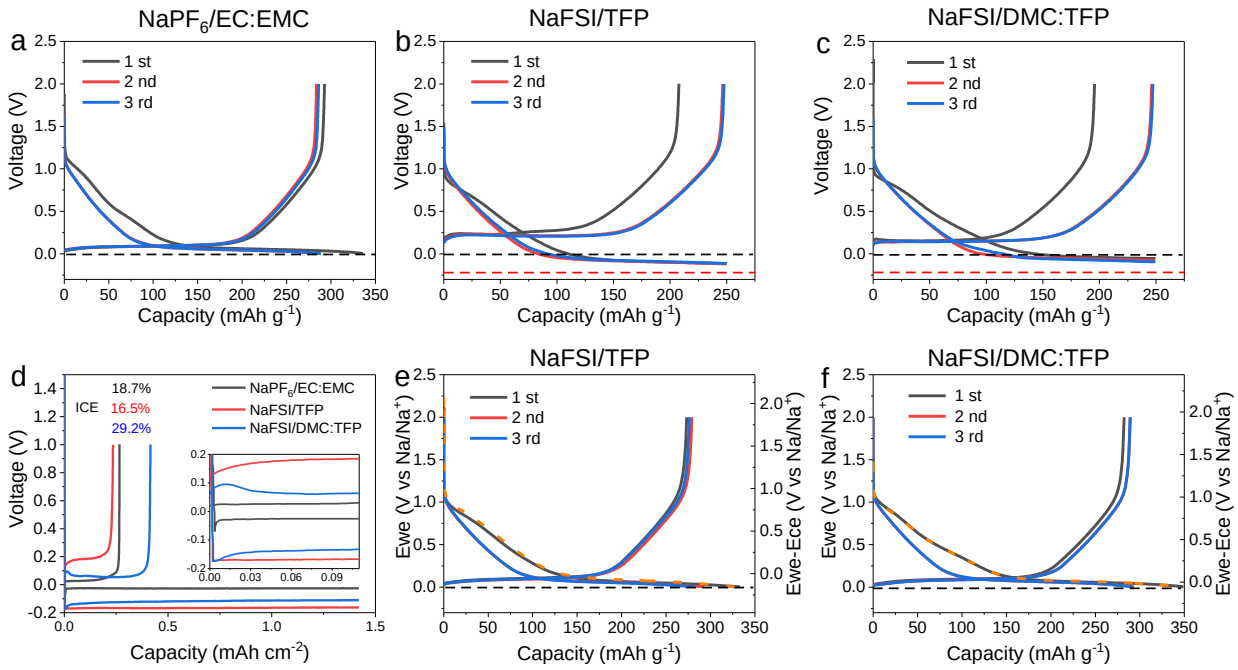

Supplementary Figure 20 | HC anode performance. a-c, the charge−discharge voltage curves of initial three cycles for HC presodiation in the Na||HC two-electrode half-coin cells using $NaPF_6$/EC:EMC (a), NaFSI/TFP (b), NaFSI/DMC:TFP (c) electrolytes. The black dash lines are 0 V and red dash lines in b and c are overpotential voltages of Na metal deposition (observed at the onset of Na metal plating from Supplementary Fig. 20d). d, voltage curves of Cu||Na cells at a current density of 0.17 mA cm^{-2} and capacity of 1.42 mAh cm^{-2} (the same values for HC presodiation in Supplementary Fig. 20a-c). Inset are the enlarged curves. e-f, the charge−discharge voltage curves of initial three cycles of HC in three-electrode cells (WE: HC, CE: Na, RE: Na) using NaFSI/TFP (e), NaFSI/DMC:TFP (f) electrolytes. The black dash lines are 0 V of E_{we} and orange dash lines are E_{we}-E_{ce} voltage-capacity curves corresponding to the right axis.

Supplementary Note 10 | Pre-sodiation experiment of HC was performed in Na||HC cells for 3 cycles at 0.1 C (1 C=300 mAh g^{-1}) to increase initial CE of HC||NaNMC full cell. The HC half

cells were disassembled at the de-sodiation state and assembled with fresh NaNMC cathode for the full cell. In $NaPF_6$/EC:EMC electrolyte, the discharge/charge process was cycled in the voltage range of 5 mV - 2 V. For NaFSI/TFP and NaFSI/DMC:TFP electrolytes, the discharge process was ended by capacity limit of 250 mAh g^{-1}, while charge process was ended at 2 V. The larger polarization of HC||Na coin cells in both NaFSI/TFP (b) and NaFSI/DMC:TFP (c) electrolytes is resulted by the overpotential of Na metal rather than HC itself. The overpotential of Na metal deposition in TFP based electrolyte (-0.17 V) was larger than baseline carbonate electrolyte (-0.07 V), proved by Cu||Na coin cells (d).

The three-electrode HC half-cells (WE: HC, CE: Na, RE: Na) were tested to demonstrate the real HC electrochemical performance, including discharge and charge capacity, and voltage of HC working electrode versus Na metal reference electrode. The three-electrode cell was tested in the working electrode voltage (Ewe) range of 0.005-2 V at 0.1 C (1C=300 mAh g^{-1}). The charge and discharge curves for the initial 3 cycles are presented in Supplementary Fig. 20 e-f in NaFSI/TFP and NaFSI/DMC:TFP electrolytes. In NaFSI/DMC:TFP electrolyte, the first discharge and charge capacity is 349 and 282 mAh g^{-1}, with 81% ICE. The discharge capacity at the second and third cycle is always large than 290 mAh g^{-1}. So, we choose 250 mAh g^{-1} as the limit capacity for Na insertion during HC presodiation in two-electrode coin cells to avoid Na metal deposition (Supplementary Fig. 20b-c). Besides, even though the HC two-electrode coin cell voltages (corresponding to Ewe-Ece in three-electrode cells configurations, right axis in Supplementary Fig. 20e-f) go down 0 V in Supplementary Fig. 20b-c, real HC WE voltage (Ewe in three-electrode cell configurations, left right axis in Supplementary Fig. 20e-f) is still above 0 V without Na metal deposition.

Supplementary Table 1 | The density, mole concentration and ionic conductivity (at 30 ℃) of the electrolytes studied in this work.

Electrolyte composition	Density ($g\ ml^{-1}$)	Mole concentration	Ionic conductivity ($mS\ cm^{-1}$)
1 M $NaPF_6$/EC:EMC (3:7 in vol)	1.22	1 M	10.13
1 M NaFSI/TFP	1.64	1 M	0.59
1.5 M NaFSI/DMC:TFP (1.5:2 in mole or 1.6:8.4 in wt.)	1.58	1.5 M	1.43

Supplementary Table 2 | Fitting electrolyte resistance (R_e) and interfacial resistance ($R_{interfacial}$) of HC||NaNMC cells using $NaPF_6$/EC:EMC, NaFSI/TFP and NaFSI/DMC:TFP electrolytes after the 3rd cycle and the 100th cycle.

Electrolyte	3^{rd} cycle resistance (Ω)		100^{th} cycle resistance (Ω)	
	R_e	$R_{interfacial}$	R_e	$R_{interfacial}$
1 M $NaPF_6$/EC:EMC (3:7 in vol)	3.97	584.15	2.43	2082.12
1 M NaFSI/TFP	26.40	444.14	20.37	338.47
1.5 M NaFSI/DMC:TFP (1.5:2 in mole or 1.6:8.4 in wt.)	10.77	281.22	9.94	232.23

Supplementary Note 11 | The electrolyte resistance and interfacial resistance values were estimated from the impedance spectra shown in Supplementary Fig. 8 and summarized in Supplementary Table 2. The intercept of the high frequency response with the real axis is the electrolyte resistance (R_e). The intermediate-to-high-frequency semicircles are related to the charge transfer resistance (R_{ct}) in the electrode/electrolyte interphase and SEI layer resistance (R_{sf}) of the passivation surface film. The total of R_{ct} and R_{sf} is considered as the interfacial resistance ($R_{interfacial}$).

Supplementary Note 12 | Supplementary Methods

Electrochemical test: Electrochemical impedance spectra (EIS) were performed on Bio-Logic Instruments (VSP) in the frequency range of 1 M-0.005 HZ with 5 mV perturbation.

Characterization: Ionic conductivity was measured by the Biologic MCS 10 system in the temperature range from -20 to 60 °C. The cell constants were evaluated using standard solutions from Oakton. The viscosity of the electrolytes as a function of temperature was measured with an Anton Paar rheometer (MCR-101; Ashland, VA, USA). A DG26.7 SS measuring system coupled with a C-PTD200 cell was used. A Peltier system installed in the measuring system was employed for temperature control. Before the sample measurement, a performance check was conducted to the rheometer and measuring system using de-ionized water (DIW) at 20˚C as a check standard. The measured values were compared to the real viscosity value of DIW at 20˚C to evaluate the performance of the system. To test the viscosity change over temperature, a temperature ramp was applied to the electrolyte samples during measurements. The temperature was set at 0˚C to start the measurements. Once a measurement was started, temperature was increased linearly with time from 0˚C to 60˚C in a duration of 45 min while the viscosity was measured and recorded with the values logged in every 30 sec. Shear rate of 50 1/s was used for all measurements. After each sample measurement, the DG26.7 measuring system was dissembled for washing and drying, and then reassembled for a new sample. A nitrogen flow through the measuring system was established to minimize the sample exposure to air. Flammability test was conducted by igniting the glass fiber absorbed 100 μL electrolyte and leaving it for self-extinguish. The self-extinguish time (SET) was calculated by dividing the burning time to the electrolyte weight. For the XPS characterization for the series of the pristine electrodes in Supplementary Fig.13-15, three kinds of electrodes were analyzed as the comparation. One is the pristine electrodes; the others are the solvent-soaked

electrodes (soaking the pristine electrodes in DMC:TFP solvent for 50 h) and electrolyte-soaked electrodes (soaking the pristine electrodes in NaFSI/DMC:TFP electrolyte for 50 h).

Gas generation test: For the in situ differential electrochemical mass spectrometry (DEMS) measurement, the EC-cell was assembled with fresh NaNMC cathode (12.6 mm diameter with needle pierced holes for gas flow), fresh HC anode (15 mm diameter), GF/B separator and 400 μl electrolyte in an Ar- filled glove box. The mass of NaNMC cathode and HC anode is around 9.2 mg and 9 mg (active materials only), respectively. The HC was not presodiated to get the gas evolution during the initial formation cycle. The electrochemical measurement was controlled by Biologic via a constant current at 0.1 C (1 C= 200 mAh g^{-1}) in the voltage range of 1.2-4.2 V. The generated gas was carried out by the carrier Ar gas and detected by a quadrupole mass spectrometer (Hiden Analytica). The cell was purged by Ar for 30 min to remove the contaminations before test. Typical m/z ratios were recorded to follow evolution of possible gases including H_2: m/z = 2, F_2: m/z = 38, Ar: m/z = 40, CO_2: m/z = 44, SO_2: m/z = 64, CF_3: m/z = 69, CH_2CF_3: m/z = 83. The DEMS signal data of pressure (Torr) were automatically outputted. The gas generation rate inside the cell with different electrolytes was compared by normalized intensity ($Torr_{target\ gas}/Torr_{Ar}$).

Supplementary References

1. Eshetu, G. G. et al. Comprehensive insights into the reactivity of electrolytes based on sodium ions. *ChemSusChem* **9**, 462-471 (2016).

2 Westman, K. et al. Diglyme based electrolytes for sodium-ion batteries. *ACS Appl. Energy Mater.* **1**, 2671-2680 (2018).

3 Konarov, A., Kim, H. J., Yashiro, H. & Myung, S.-T. Passivation of aluminum current collectors in non-aqueous carbonate solutions containing sodium or potassium hexafluorophosphate salts. *J. Mater. Chem. A* **7**, 13012-13018 (2019).

4 Björklund, E., Göttlinger, M., Edström, K., Brandell, D. & Younesi, R. Investigation of Dimethyl Carbonate and Propylene Carbonate Mixtures for LiNi0. 6Mn0. 2Co0. 2O2‐Li4Ti5O12 Cells. *ChemElectroChem* **6**, 3429-3436 (2019).

5 Metzger, M., Strehle, B., Solchenbach, S. & Gasteiger, H. A. Origin of H_2 evolution in LIBs: H_2O reduction vs. electrolyte oxidation. *J. Electrochem. Soc.* **163**, A798- A809 (2016).

6 Zhang, L., Tsolakidou, C., Mariyappan, S., Tarascon, J.-M. & Trabesinger, S. Unraveling gas evolution in sodium batteries by online electrochemical mass spectrometry. *Energy Storage Mater.* **42**, 12-21 (2021).